Coherent x radiation induced by relativistic electrons in crystals

V. B. Gavrikov,[1] V. P. Likhachev,[2] and J. D. T. Arruda-Neto[2,3]
[1]*Kharkov Institute of Physics and Technology, 1 Akademishna, 61108 Kharkov, Ukraine*
[2]*Instituto de Física da Universidade de São Paulo, CP66318, 05315-970 São Paulo, SP, Brazil*
[3]*University of Santo Amaro/UNISA, São Paulo, SP, Brazil*
(Received 19 April 2003; published 28 August 2003)

We present the results of a theoretical study of coherent x radiation induced by relativistic electrons in crystals for observation angles exceeding γ^{-1}, where γ is the projectile Lorentz factor. The assumption for the process includes both elastic and inelastic radiation mechanisms. The results were compared with available experimental data.

DOI: 10.1103/PhysRevA.68.024901 PACS number(s): 79.20.Kz, 41.75.Ht, 78.70.Ck

Up to now, several theoretical approaches for the coherent x-radiation description, based on classical electrodynamics [1–3] and quantum theory [4,5], have appeared. In these approaches, the emission of coherent photons was reduced to the process of elastic scattering of virtual photons associated with the projectile, on bound crystal electrons. Such approaches correspond to the form-factor approximation used in the theory of Rayleigh scattering of real photons by an isolated atom [9] and therefore, it cannot give a full description of the process, which is achieved by taking into account the inelastic channel.

In our recent works [6,7], we studied differential and integral properties of incoherent x radiation, using the radiation amplitude of Amus'ya *et al.* [8] for the case of interaction between a relativistic projectile and an isolated nonrelativistic atom, and considered two channels leading to the radiation by crystal electrons: elastic channel when states of the crystal target before and after radiation process are identical, and inelastic channel when in the final state the target emits one of its electrons.

It was shown that at observation angles $\theta_\gamma > 10\gamma^{-1}$ (γ is the projectile Lorentz factor), the crystal electrons provide a dominant contribution to the total radiation yield.

In the present work, we used the same approach as in Ref. [6,7] to obtain, for photon energies $\omega \ll m$, where m is the electron mass, the total coherent cross section, taking into account both the elastic and the inelastic radiation channels, and then compared our results with available experimental results.

Let us consider a photon with energy ω and wave vector $\vec{k}$, which lies within a solid angle $d\Omega_\gamma$ around θ_γ, resulting from the passage of an electron with initial energy E_1, momentum $\vec{p}_1$, and velocity $\vec{v}_1$ through a set of crystallographic planes with a reciprocal lattice vector $\vec{g}$. After interaction, the outgoing electron with energy E_2 and momentum $\vec{p}_2$ moves within a solid angle $d\Omega_{p_2}$ around $\vec{p}_2$. During the radiation, the medium acquires momentum $\vec{q}=\vec{p}_1-\vec{p}_2-\vec{k}$ and the momentum-energy relationship $p^2=E^2-m^2$ is always valid.

As in the theory of high-energy coherent bremsstrahlung [10,11], the coherent cross section can be presented as a product of a radiation cross section for an isolated atom $d\sigma_{at}$ and the coherent diffraction factor f_{coh}, in the form

$$d\sigma_{coh}=f_{coh}d\sigma_{at}=\frac{(2\pi)^3}{VN}D_T|D(\vec{g})|^2\delta(\vec{q}-\vec{g})d\sigma_{at}, \quad (1)$$

where $d\sigma \equiv d^5\sigma/d\omega d\Omega_\gamma d\Omega_{p_2}$, and it is assumed that there is no overlap of terms with different $\vec{g}$ in the radiation pattern. In Eq. (1), V is the volume of the unit crystal cell; N is the number of atoms per unit cell; and $|D(\vec{g})|^2$ is the crystal structure factor, $D(\vec{g})=\Sigma_i \exp(i\vec{g}\cdot\vec{r}_i)$, where $\vec{r}_i$ describes the position of the ith atom within the cell. For the diamond-type structure ($N=8$) considered here, the structure factor is

$$|D(\vec{g})|^2=\left[1+\exp\left(i\frac{\pi}{2}(h+k+l)\right)\right]\times[1+(-1)^{h+k}+(-1)^{h+l}+(-1)^{k+l}], \quad (2)$$

where h,k, and l are the Miller indices of the planes and therefore, $|D(\vec{g})|^2$ is (a) equal to 64 for all planes with even indexes and their sum is a multiple of 4; (b) equal to 32 if all the indexes are odd; and (c) otherwise equal to zero . The δ function in Eq. (1) reflects the fact that the coherent cross section can be essential only when the momentum transferred is very close to that of a reciprocal lattice vector. The incoherent factor D_T takes into account disorder in the reciprocal location of different crystal atoms.

From the condition $\vec{q}=\vec{g}$, one can get the energy dependence of coherent photons on θ_γ and the reciprocal orientation of $\vec{v}_1$ and $\vec{g}$:

$$\omega_{coh}=\frac{gv_1\sin\varphi-\frac{g^2}{2E_1}}{1-v_1\cos\theta_\gamma+\frac{g}{E_1}\sin\theta_1}, \quad (3)$$

where φ is the angle between the crystal planes and $\vec{v}_1$ and $\theta_1=\theta_\gamma+\varphi$. In the case of $E_1 \gg g$, Eq. (3) coincides with an accuracy of terms of order g/E_1 with the high-energy limit result [12,13]. In this limit and for $\theta_\gamma > \gamma^{-1}$, the dependence of ω_{coh} on γ is negligible.

As in the case of incoherent radiation ([6,7]), the coherent cross section in Eq. (1) consists of elastic and inelastic parts. The elastic cross section describes the interaction of the projectile with an atom as a whole and it is a sum of the static (Bethe-Heitler) cross section $d\sigma_{st}$, the polarization cross section $d\sigma_{pol}$, and the interference term $d\sigma_{int}$. For the elastic channel, D_T [Eq. (1)] is caused by the thermal disorder in a crystal and therefore, it has to be replaced by the Debye-Waller factor $D_T^{el}=\exp(-g^2u^2)$ [11,14], where u^2 is the mean-square temperature displacement of the atoms from their equilibrium positions.

The inelastic channel results from the interaction of the projectile with atomic electrons as individual particles. The inelastic cross section is a sum of $d\sigma_{com}$, the cross section describing Compton scattering of virtual photons associated with the projectile by the bound electrons, and $d\sigma_{rel}$, the cross section due to the radiation of the projectile in the field of the atomic electrons. While the elastic cross sections assume statical distributions of the electron clouds surrounding the nuclei of the crystal atoms, for the inelastic contributions, an instantaneous straggling in positions of electrons belonging to different crystal atoms plays an essential role. Assuming that the average value of this straggling is equal to a screening (Thomas-Fermi) radius $a=0.885a_0Z^{-1/3}$, where a_0 is the Bohr radius and Z is the atomic number of the crystal, factor D_T for the inelastic channel should be replaced by $D_T^{inel}=\exp[-g^2(u^2+a^2)]$.

Thus, the coherent cross section can be recast in the form

$$d\sigma_{coh}=D_T^{el}d\sigma_{coh}^{el}+D_T^{inel}d\sigma_{coh}^{inel}, \tag{4}$$

where the elastic contribution $d\sigma_{coh}^{el}$ is

$$d\sigma_{coh}^{el}=d\sigma_{st}+d\sigma_{pol}+d\sigma_{int} \tag{5}$$

and the inelastic contribution is

$$d\sigma_{coh}^{inel}=d\sigma_{com}+d\sigma_{rel}. \tag{6}$$

By assuming that (1) $\omega \ll E_1,E_2$, $\omega \ll m$; (2) $q \ll p_1,p_2$; and (3) all radiation energies are large compared to those of electronic binding, and using the δ function in Eq. (1) to integrate over $d\omega$ and $d\Omega_{p_2}$, one can find that in the laboratory coordinate system and in the case when vectors $\vec{k},\vec{p}_1$, and $\vec{g}$ lie in the same plane, the components of the total cross section have the form ($d\sigma \equiv d^2\sigma/d\Omega_\gamma$)

$$\begin{aligned} d\sigma_{st}&=\sigma_0Z^2[1-F(g)]^2T_1,\\ d\sigma_{pol}&=\sigma_0Z^2F^2(g)T_2,\\ d\sigma_{int}&=2\sigma_0Z^2F(g)[1-F(g)]T_3, \end{aligned} \tag{7}$$

where

$$T_1=\left[\frac{1}{\gamma}\frac{\cos\theta_2}{1-v_1\cos\theta_\gamma}\right]^2,$$

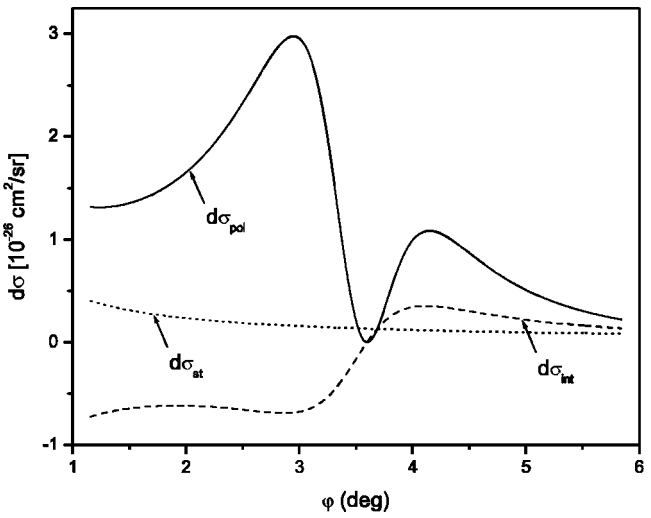

FIG. 1. The elastic cross sections as a function of φ for the (111) planes of a silicon crystal at $\theta_\gamma=7°$ and $E_1=25$ MeV. The $d\sigma_{com}$ contributes to the total cross section as 3.3% of $d\sigma_{pol}$ and the contribution of $d\sigma_{rel}$ is 36.1% of $d\sigma_{st}$.

$$T_2=\left[\frac{v_1\cos\theta_\gamma(\cos\theta_2-v_1\cos\varphi)-\gamma^{-2}\cos\theta_2}{1-v_1\cos(\theta_2-\varphi)}\right]^2, \tag{8}$$

$$T_3=\frac{1}{\gamma}\frac{\cos\theta_2}{1-v_1\cos\theta_\gamma}\times\frac{v_1\cos\theta_\gamma(\cos\theta_2-v_1\cos\varphi)-\gamma^{-2}\cos\theta_2}{1-v_1\cos(\theta_2-\varphi)}.$$

In Eqs. (8), $\theta_2=\theta_\gamma-\varphi$, $\sigma_0=(8\pi^2/VN)(\alpha r_e^2/\omega_{coh}g^2)|D(\vec{g})|^2$, $\alpha=1/137$, and r_e is the classical electron radius. The components of the inelastic part of the total cross section are

$$d\sigma_{com}=\sigma_0Z^2S(g)T_2, \tag{9}$$

$$d\sigma_{rel}=\sigma_0Z^2S(g)T_1. \tag{10}$$

In Eqs. (7) and (9), $F(g)$ is the atomic form factor and $S(g)$ is the incoherent-scattering function [15,16].

The angular dependence of the elastic cross section components on φ is shown in Fig. 1 for $\theta_\gamma=7°$, $E_1=25$ MeV, and for the case when the radiation is generated on the (111) planes of a silicon crystal. It is seen from this figure that the main contributions to the total cross section come from $d\sigma_{pol}$ and $d\sigma_{int}$. $d\sigma_{pol}$ has two maxima at $\varphi^{(\pm)}=\theta_\gamma/2 \pm 1/2\gamma$ and a minimum at $\varphi_0=(\theta_\gamma/2)+(\coth\theta_\gamma/2/4\gamma^2\cos\theta_\gamma)$ [13,17]. The interference contribution changes its sign at $\varphi=\varphi_0$. For the case of relativistic positrons, $d\sigma_{int}$ has the opposite sign. For the chosen crystal and planes, the ratio between $d\sigma_{pol}$ and $d\sigma_{com}$ is 30.3 and for $d\sigma_{st}$ and $d\sigma_{rel}$, the ratio is 2.77.

The comparison between the available experimental data and our calculations is presented in Figs. 2–4. In the calculations, we assumed crystal targets were kept at room temperature. It should be noted that the data presented in the literature, on experimental investigations of coherent x radia-

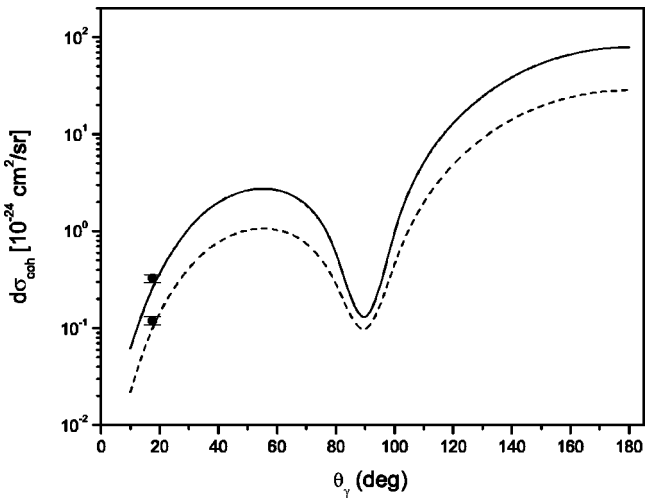

FIG. 2. The coherent cross section as a function of θ_γ at $E_1=25$ (solid line) and 15 (dashed line) MeV for the (111) planes of a silicon crystal. The data are taken from Ref. [18].

tion, are reported in the form of photon fluxes (per incident particle or per one incident particle and one steradian) and not as radiation cross sections. Because of this, we show in Figs. 3 and 4 the ratios for calculated and measured values.

In Fig. 2 the maximal values of the coherent cross sections at fixed θ_γ are presented as functions of θ_γ for a silicon crystal. The radiation is generated in the (111) planes by electrons with $E_1=25$ MeV (solid line) and $E_1=15$ MeV

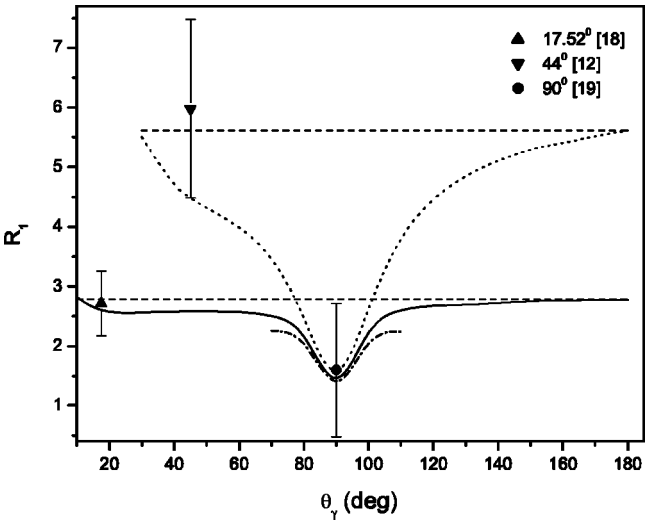

FIG. 3. The ratio between coherent cross sections at different projectile energies and for those φ where these cross sections are maximal [Eq. (11)]. The solid curve corresponds to R_1 for the (111) planes of a silicon crystal at $E_1=25$ MeV and $E_1'=15$ MeV. The dotted curve shows (111) planes of a diamond crystal at $E_1=8.3$ MeV and $E_1'=3.5$ MeV. The dash-dotted curve shows R_1 near $\theta_\gamma=90°$ for the (800) planes of a diamond crystal at $E_1=900$ MeV and $E_1'=600$ MeV. The datum (circle) is taken from Ref. [19] ($\theta_\gamma=90°$). The dashed lines correspond to the dependence of radiation intensity versus projectile energy as γ^2, predicted in Ref. [12], for two ratios of energies (25/15 and 8.3/3.5). Angles refer to the experimental observation angles.

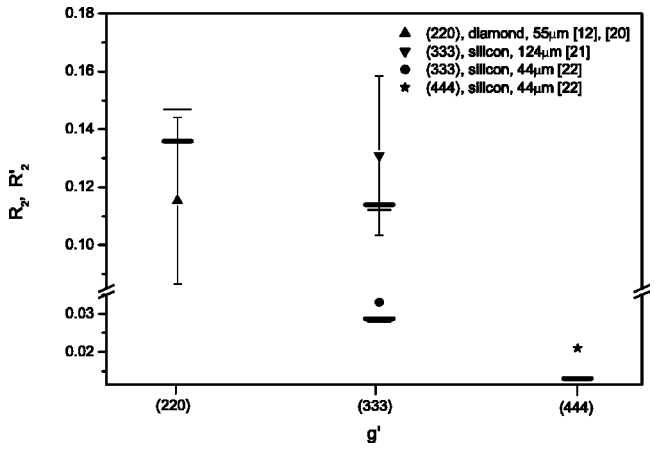

FIG. 4. Comparison of the present calculations for R_2 [Eq. (12)], and R_2' [Eq. (13)] for g corresponding to (111) crystal planes, with experimentally defined ratios between the intensities of the coherent radiation generated on different crystal planes. Inserted in the upper-right corner are the plane indexes, type of the crystals, and thicknesses.

(dashed line). The experimental data are taken from our previous work [18], where the observation angle was 17.52°. It is seen that $d\sigma_{coh}$ has a minimum at $\theta_\gamma=90°$ and, as for the incoherent cross section [6], achieves its maximal values near $\theta_\gamma=180°$.

In Fig. 3, we show the ratio of the cross sections for two projectile energies:

$$R_1=\frac{d\sigma_{coh}(E_1)}{d\sigma_{coh}(E_1')} \tag{11}$$

as a function of θ_γ. As in Fig. 2, we consider here the maximal values of $d\sigma_{coh}$ at each θ_γ. The solid line presents R_1 for the case when the radiation is generated by the (111) planes of a silicon crystal at $E_1=25$ MeV and $E_1'=15$ MeV; the experimental datum (triangle up) is taken from Ref. [18]. The dotted line shows the ratio for the (111) planes of a diamond crystal at $E_1=8.3$ MeV and $E_1'=3.5$ MeV; the experimental data (triangle down) are from Ref. [12] ($\theta_\gamma=44°$). The dash dotted line shows R_1 near $\theta_\gamma=90°$ for the (800) planes of a diamond crystal at $E_1=900$ MeV and $E_1'=600$ MeV. The datum (circle) is taken from Ref. [19] ($\theta_\gamma=90°$). The dashed lines correspond to the dependence of radiation intensity versus projectile energy as γ^2, predicted in Ref. [12] for two ratios of projectile energies (25/15 and 8.3/3.5). As shown in the figure, our R_1 has a minimum at $\theta_\gamma=90°$ and reaches the predicted value only near the forward and backward observation directions.

A contribution of the inelastic radiation channel to $d\sigma_{coh}$ is small and more appreciable for low-Z crystals, and for those planes having low Miller indices. Indeed, for the middle- and high-Z crystals and low plane indices, $S(g)$ can be neglected in comparison with $F^2(g)$, and for higher plane indices the inelastic contribution is strongly reduced by a factor D_2.

In Fig. 4, we compare another calculated ratio, namely,

$$R_2=\frac{f(\omega_{coh})}{f(\omega'_{coh})}\frac{d\sigma_{coh}(g)}{d\sigma_{coh}(g')}, \tag{12}$$

with the ratio from the experimental data. In Eq. (12), the cross sections are taken at the maximum of their angular distributions; g corresponds to (111) crystal planes and the attenuation factor is $f(\omega)=L_a^{-1}[1-\exp(-L_a^{-1}t)]$, where L_a is the absorption length at a given photon energy, and t is the target thickness. In Fig. 4, R_2 is represented by thick horizontal lines and the thin horizontal lines show the ratio for elastic contribution:

$$R'_2=\frac{f(\omega_{coh})}{f(\omega'_{coh})}\frac{d\sigma^{el}_{coh}(g)}{d\sigma^{el}_{coh}(g')}. \tag{13}$$

For g' corresponding to the (220) plane, the ration is shown for a diamond crystal. The experimental ratio (triangle up) was defined by using the data from Ref. [12] for the (111) plane and from [20] for the (220) plane. For the (333) and (444) plane indexes the calculated ratios are shown for a silicon crystal. The experimental ratios were defined from the data presented in Ref. [21] (triangle down) and in Ref. [22] (circle and star); experimental errors in Ref. [22] are not reported. In the calculations, we take into account the attenuation of the photon flux inside the targets by using the data from Ref. [23]. Note that while for the (220) case the difference between R_2 and R'_2 is about 7.5%, for the (333) planes it is less than 1.5%.

As follows from above, the coherent cross section Eq. (4) is in satisfactory agreement with the experimental data known up to now. The delineation of relative contributions from elastic and inelastic mechanisms to the total radiation yield requires more precise experiments. The results obtained in this work, together with the results of Refs. [6,7], can be used in the planning of more detailed experimental investigations of the process by using coincidence techniques, as well as for investigations of the radiation processes induced by relativistic particles where the considered radiation appears as a background effect.

[1] D. Dialetis, Phys. Rev. **17**, 1113 (1978).
[2] I.D. Feranchuk and A.V. Ivashin, J. Phys. (Paris) **46**, 1981 (1985).
[3] X. Artru and P. Rullhusen, Nucl. Instrum. Methods Phys. Res. B **145**, 1 (1998).
[4] H. Nitta, Phys. Rev. B **45**, 7621 (1992).
[5] H. Nitta, Nucl. Instrum. Methods Phys. Res. B **115**, 401 (1996).
[6] V.B. Gavrikov *et al.*, Phys. Rev. A **65**, 022903 (2002).
[7] V.B. Gavrikov *et al.*, Eur. Phys. J. A **12**, 487 (2001).
[8] M. Ya. Amus'ya *et al.*, in *Polarization Bremsstrahlung*, edited by V.N. Tsytovich and I.M. Oiringel (Plenum, New York, 1992), Chap. 5.
[9] The form factor approximation was discussed in detail by L. Kissel *et al.*, Phys. Rev. A **22**, 1970 (1980).
[10] M.L. Ter Mikaelyan, Zh. Eksp. Teor. Fiz. **25**, 296 (1953).
[11] H. Uberall, Phys. Rev. **103**, 1055 (1956).
[12] J. Freudenberger, *et al.*, Phys. Rev. Lett. **74**, 2487 (1995).
[13] V.B. Gavrikov *et al.*, Braz. J. Phys. **29**, 516 (1999).
[14] L.I. Schiff, Phys. Rev. **117**, 1394 (1960).
[15] J.H. Hubbell *et al.*, J. Phys. Chem. Ref. Data **4**, 471 (1975).
[16] R. Ribberfors and K.-F. Berggren, Phys. Rev. A **26**, 3325 (1982).
[17] V.B. Gavrikov *et al.*, Nucl. Instrum. Methods Phys. Res. A **457**, 411 (2001).
[18] D.I. Adejishvili *et al.*, Nucl. Instrum. Methods Phys. Res. B **152**, 406 (1999).
[19] S.A. Vorobiev *et al.*, JETP Lett. **41**, 1 (1985).
[20] J. Freudenberger *et al.*, Nucl. Instrum. Methods Phys. Res. B **119**, 123 (1996).
[21] K.-H. Brenzinger *et al.*, Z. Phys. A: Hadrons Nucl. **358**, 107 (1997).
[22] R.B. Fiorito *et al.*, Phys. Rev. Lett. **71**, 704 (1993).
[23] B.L. Henke *et al.*, At. Data Nucl. Data Tables **54**, 181 (1993).